Detection and Localization of Defects in Cable Sheath of Cross-Bonding Configuration by Sheath Currents

Marina Adel Shokry, Abderrahim Khamlichi, Fernando Garnacho, Julio Martínez Malo, and Fernando Álvarez

***Abstract*—Nowadays, many researchers are focusing on on-line condition monitoring of high-voltage insulated cable systems to prevent failures. With the aim of reducing the voltage induced in the cable sheaths, cross-bonding (CB) grounding cable systems are used in long distance power transmission land lines. This paper proposes a new criterion for the detection and localization of defects that might occur in the cable sheath when a CB configuration is adopted. The proposed criterion can be applied at different levels of load current. For the application of the criterion, the cable system under evaluation is modeled using the alternative transient program (ATP) software. Various practical cases were studied, showing the effectiveness of the criterion for the detection and localization of different types of defects in simulated cable systems. Furthermore, in order to validate the criteria adopted for the defect detection, based on the ATP model, a real defected case was evaluated. The results obtained proved that this criterion is suitable for the detection and localization of defects in the cable sheaths, when on-line measurements are performed in monitoring applications.**

***Index Terms*—Condition monitoring, current measurements, electric breakdown, cable shielding, sheath current, fault current.**

I. Introduction

HV INSULATED power cables form an essential part in the distribution and transmission network grids in the urban areas due to their high reliability, environmental friendliness and visual impact. Although the life time of insulated power cables may exceed 30 years, if proper start-up and maintenance policies are not carried out, this period can be considerably reduced. Thus, on-line diagnostic techniques are becoming commonly applied on HV and MV power grids.

For utilities, the main advantage of performing on-line measurements for the assessment of the cable sheath condition is that the interruption of the power supply is not required, while in off-line measurements a planned shutdown is needed [1]–[4].

In short underground cable systems and in submarine cable systems, solid bonding sheath connections are usually applied [5], [6]. However, in long underground cables, Cross Bonding (CB) configuration or a combination between CB and Single point (SP) are usually used to reduce the induced current in the cable sheaths in order to avoid losses in cable sheath [5]–[8].

The sheath currents depend on the asymmetry of the load currents, the laying methods, the length of the minor sections and the external electromagnetic field [5]. In the studies presented in [9], [10], the reasons that originate failures in power cables are classified into 6 groups; adverse environmental conditions, poor workmanship, manufacturing problems, operational or maintenance reasons and age degradation. Some cable defects cause excessive sheath current like faults, breakdown between sheaths and flooding in linkboxes [1], [2], [11].The feasibility of detecting a fault in the cable over-sheath by monitoring the sheath currents to ground at the end of the cross-bonded sections is presented in [4]. A method has been developed by Mingzhen Li *et al.* to detect and localize faults in CB configuration by monitoring sheath currents [2].

Different criteria (depending on the type of the defect) were developed by Xiang Dong *et al.* [1] to detect defects in cable sheaths by measuring sheath currents when CB configurations without transposition in flat formation are adopted. Although this study is very efficient to detect the defects in cable sheaths, the influence of the load current and the unbalance of the lengths of the minor sections have not been studied on the criteria proposed. Moreover, the feasibility of detecting sheath defects by measuring sheath currents on the CB configuration with cable transposition have not studied before.

This paper presents a generic novel criterion for detecting and localizing defects in the cable sheaths: open circuit in sheath loop, breakdown between sectionalized sheaths, inadequate sheath connection in linkbox and flooding in linkbox, for CB with and without transposition, for any percentage of load currents. Simple codes from #0 to #4 are introduced to represent the degree of change of the sheath current in case of a defect. Furthermore, in this criterion the influence of the cable formation type (in trefoil or flat) and the unbalance in CB minor sections are considered. In addition, the criterion has been improved by subtracting the capacitive component of the sheath current

Manuscript received October 9, 2018; revised January 29, 2019; accepted February 25, 2019. Date of publication March 6, 2019; date of current version July 23, 2019. This work was supported by the European Union's Horizon 2020 research and innovation programme under the Marie Sklodowska-Curie innovation training network, under Grant 676042, titled MEAN4SG. Paper no. TPWRD-01081-2018. *(Corresponding author: Marina Adel Shokry.)*

M. A. Shokry, A. Khamlichi, J. M. Malo, and F. Álvarez are with the Universidad Politécnica de Madrid, 28040 Madrid, Spain (e-mail: madel@lcoe.etsii.upm.es; ak@lcoe.etsii.upm.es; julio.martinezm@upm.es; fernando.alvarez@upm.es).

F. Garnacho is with the Laboratorio Central Oficial de Electrotecnia, Fundación Para el Fomento de la Innovación Industrial, 28906 Madrid, Spain (e-mail: fgarnacho@lcoe.etsii.upm.es).

Color versions of one or more of the figures in this paper are available online at http://ieeexplore.ieee.org.

Digital Object Identifier 10.1109/TPWRD.2019.2903329

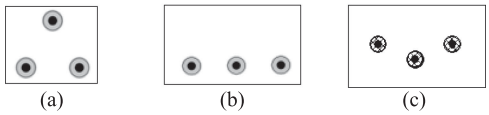

Fig. 1. Cable laying configuration. (a) Trefoil formation. (b) Flat formation (c) Semi-trefoil formation.

to validate the proposed criterion under low levels of load current.

II. Problem Statement

This section is divided into 4 sub-sections. The first subsection, the types of CB configurations and the analytical equations used for calculating the sheath current in CB with transposition under normal condition are explained. In the second subsection, the alternative transient program (ATP) software cable model is presented Furthermore; a comparison is performed between the results obtained from the programed Matlab code based on the analytical equations and those obtained from the ATP software. In the third subsections, the proposed criterion for the detection of defects is explained. Finally, in the fourth sub-section, a complementary method is discussed in order to validate the proposed method under low levels of load currents.

A. Theoretical Equations

A CB configuration is formed by 3 minor sections. Ideally the three sections should have the same length (balanced CB), however, in practice, they may slightly differ in length (L_1, L_2, and L_3); nevertheless, the difference in lengths should not be higher than 30% in any case, in order to reduce losses [5]. In each minor section, three single phase cables of equal lengths are installed. There are two types of configuration for cable laying: trefoil formation and flat formation, as shown in Fig. 1(a) and 1(b). Sometimes due to installation conditions, the cables are inserted in ducts which might leads to a semi trefoil formation as shown in Fig. 1(c).

The CB configuration without cable transposition is used for trefoil formation (Fig. 2(a)), whereas CB with cable transposition is usually applied on flat formation (Fig. 2(b)), where the cables are transposed and the sheaths remain in their position along the cable configuration [5], [12].

Sometimes due to installation conditions, the CB without transposition is applied in flat formation as well. However it can be considered an erroneous scenario if sheaths and conductors are counter transposed as higher losses will be produced [13].

In both CB configurations, the cable sheaths of each minor section are interconnected to each other through link-boxes (LB). Fig. 3 shows the electrical scheme of a typical CB grounding system without transposition and Fig. 4 illustrates the one with transposition. Three different loops of currents (J_{l1}, J_{l2}, J_{l3}) are established by crossing the cable sheaths in each CB configuration as shown in Figs. 2, 3 and 4, while a set of three load currents J_1, J_2, J_3 passes along the three phase conductors.

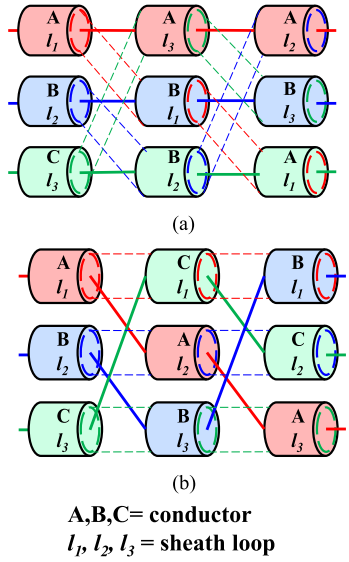

Fig. 2. (a) CB without transposition. (b) CB with transposition.

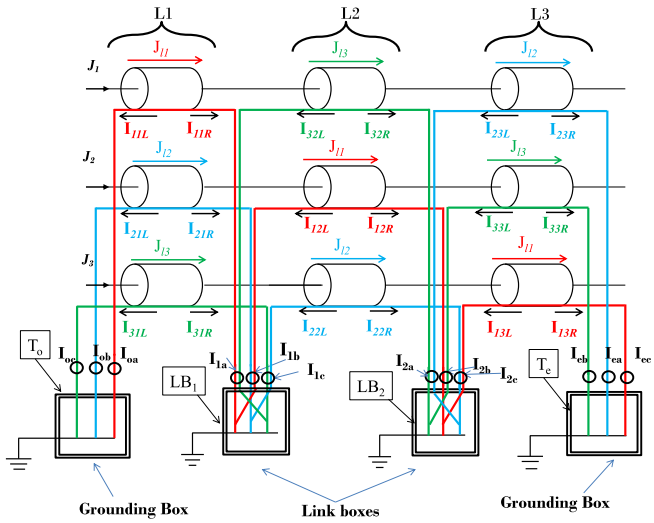

Fig. 3. CB cable system configuration without transposition.

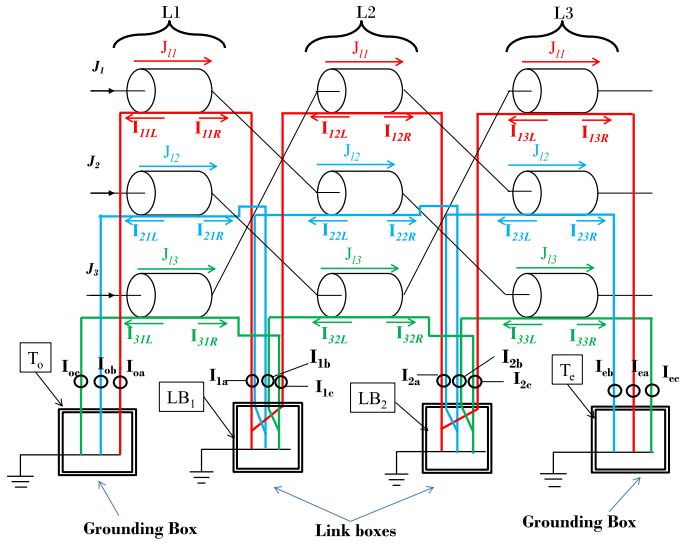

Fig. 4. CB cable system configuration with transposition.

Usually, coaxial cables are used to connect the sheaths of sectionalized cable joints to the link-boxes and unipolar cables to connect the sheath terminations of the minor sections to earth via grounding boxes.

For monitoring purposes, in both types of CB configurations current sensors can be located in 4 emplacements (see Figs. 3 and 4): at the beginning (origin) and ending terminals (sensors I_o and I_e) and at the first and the second crossing (sensors I_1 and I_2). The sensors at the terminals are fastened around unipolar cables while the sensors at link-boxes are fastened around coaxial cables. Consequently, in a CB configuration, the measured currents by sensors I_1 and I_2 are the difference between the currents of two different sheath loops.

Equation (1) shows the induced voltage in each cable sheath loop, u_{1c}, u_{2c} and u_{3c} of a CB with transposition in flat formation, due to the induced load current by the magnetic coupling between the conductors and the cable sheaths.

Where Z^{cs} is the mutual coupling impedance per unit length between a conductor and its cable sheath and Z^{cs}_{hj} is the mutual coupling impedance per unit length between the *j* cable sheath and a conductor located in the *h* laying position in a minor section in which the current is flowing. Each row of the impedance matrix [Z] multiplied by the conductor current array [*J*] represents the induced voltage due to the conductor currents per unit length in a minor section of the cable sheath loop [7].

Equation (2) shows the voltage induced in each cable sheath loop due to the self-impedance between the sheaths, where u_{1s}, u_{2s}, and u_{3s} represent the induced voltages in each loop due to the sheath loop currents (J_{l1}, J_{l2}, J_{l3}).

$$\left.\begin{aligned} u_{1c} &= \begin{bmatrix} L_1 & L_2 & L_3 \end{bmatrix} . \begin{bmatrix} Z^{cs} & Z^{cs}_{21} & Z^{cs}_{31} \\ Z^{cs}_{21} & Z^{cs}_{31} & Z^{cs} \\ Z^{cs}_{31} & Z^{cs} & Z^{cs}_{21} \end{bmatrix} \begin{bmatrix} J_1 \\ J_2 \\ J_3 \end{bmatrix} \\ u_{2c} &= \begin{bmatrix} L_1 & L_2 & L_3 \end{bmatrix} . \begin{bmatrix} Z^{cs}_{12} & Z^{cs} & Z^{cs}_{32} \\ Z^{cs} & Z^{cs}_{32} & Z^{cs}_{12} \\ Z^{cs}_{32} & Z^{cs}_{12} & Z^{cs} \end{bmatrix} \begin{bmatrix} J_1 \\ J_2 \\ J_3 \end{bmatrix} \\ u_{3c} &= \begin{bmatrix} L_1 & L_2 & L_3 \end{bmatrix} . \begin{bmatrix} Z^{cs}_{13} & Z^{cs}_{23} & Z^{cs} \\ Z^{cs}_{23} & Z^{cs} & Z^{cs}_{13} \\ Z^{cs} & Z^{cs}_{13} & Z^{cs}_{23} \end{bmatrix} \begin{bmatrix} J_1 \\ J_2 \\ J_3 \end{bmatrix} \end{aligned}\right\} \quad (1)$$

$$\left.\begin{aligned} u_{1s} &= \begin{bmatrix} L_1 & L_2 & L_3 \end{bmatrix} . \begin{bmatrix} Z^{ss} & Z^{ss}_{21} & Z^{ss}_{31} \\ Z^{ss} & Z^{ss}_{21} & Z^{ss}_{31} \\ Z^{ss} & Z^{ss}_{21} & Z^{ss}_{31} \end{bmatrix} \begin{bmatrix} J_{l1} \\ J_{l2} \\ J_{l3} \end{bmatrix} \\ u_{2s} &= \begin{bmatrix} L_1 & L_2 & L_3 \end{bmatrix} . \begin{bmatrix} Z^{ss}_{12} & Z^{ss} & Z^{ss}_{32} \\ Z^{ss}_{12} & Z^{ss} & Z^{ss}_{32} \\ Z^{ss}_{12} & Z^{ss} & Z^{ss}_{32} \end{bmatrix} \begin{bmatrix} J_{l1} \\ J_{l2} \\ J_{l3} \end{bmatrix} \\ u_{3s} &= \begin{bmatrix} L_1 & L_2 & L_3 \end{bmatrix} . \begin{bmatrix} Z^{ss}_{13} & Z^{ss}_{23} & Z^{ss} \\ Z^{ss}_{13} & Z^{ss}_{23} & Z^{ss} \\ Z^{ss}_{13} & Z^{ss}_{23} & Z^{ss} \end{bmatrix} \begin{bmatrix} J_{l1} \\ J_{l2} \\ J_{l3} \end{bmatrix} \end{aligned}\right\} \quad (2)$$

Being Z^{ss} the self-sheath impedance per unit length due to the self-coupling with its own sheath and Z^{ss}_{uv} the mutual coupling between the sheath loop *v*, in which the voltage is induced, and a different sheath loop located in the *u* position in a minor section in which the current is flowing. Each row of the impedance matrix [Z] multiplied by the cable sheath current array $[J_l]$ represents the induced voltage due to the cable sheath currents in per unit length in a minor section of the cable sheath loop.

The total induced voltage in each cable sheath u_{total} (3) provokes voltage drop in the earth resistances of both cable ends.

$$u_{total} = \begin{bmatrix} u_{1c}+u_{1s} \\ u_{2c}+u_{2s} \\ u_{3c}+u_{3s} \end{bmatrix} = -(R_1+R_2)\,.\,(J_{l1}+J_{l2}+J_{l3})\,.\begin{bmatrix} 1 \\ 1 \\ 1 \end{bmatrix} \quad (3)$$

Where R_1 and R_2 are the earth resistances.

Assuming that the capacitive current is negligible compared with the inductive one, by substituting (1) and (2) in (3), the three inductive currents J_{l1}, J_{l2} and J_{l3} are determined. However, for more precision in the sheath current calculation, the capacitive component has to be considered although the resistive current associated to the insulation resistance of the cable insulation is always assumed negligible in HV cables.

The capacitive current in HV cables is expressed by (4).

$$I_C = j.\omega.c'.U \quad (4)$$

Where:

- c' is the cable capacitance per unit length,
- U is the operating phase voltage and
- ω is the angular frequency.

The current due to the capacitive coupling depends on the total length of the CB and on the induced voltage in each minor section. The capacitive currents I_C are represented as I_{mn} where $m = 1, 2, 3$ is the number of the sheath loop and is $n = 1, 2, 3$ the number of the section. It is assumed that the capacitive component of each minor section I_{mn} is injected in the middle of its length (i.e., $L_1/2$ for the minor Section I). This capacitive component is split into two parts I_{mnR} and I_{mnL} depending on the impedance seen from each side. For instance, in minor Section I and sheath loop 1 the current is split as shown in (5) and (6).

$$I_{11R} = \frac{Z^{ss}.\frac{L_1}{2}}{Z^{ss}.(L_1+L_2+L_3)} I_{11} \quad (5)$$

$$I_{11L} = \frac{Z^{ss}.\left(\frac{L_1}{2}+L_2+L_3\right)}{Z^{ss}.(L_1+L_2+L_3)} I_{11} \quad (6)$$

Consequently the current to be measured by each sensor placed in each phase at the beginning terminal (origin), I_o, at the first and second CB, I_1 and I_2 and at the ending terminal, I_e, of the cable system, can be expressed by (7). Similarly to the process described from (1) to (7), a set of equations can be derived to determine the current to be measured by each sensor, when CB without transposition is adopted either in flat or in trefoil formation.

TABLE I
CABLE PARAMETERS

Parameters	Value
Equivalent radius of the conductor (mm)	27.6
Equivalent radius of insulation (mm)	51.9
Equivalent relative permittivity of insulation	3.08
External sheath raduis (mm)	57.25
Internal sheath raduis (mm)	54.84
Equivalent sheath resistivity at 80ºC (Ω·m)	$7.2034.10^{-8}$
Equivalent conductor resistivity at 90ºC (Ω·m)	$2.2952.10^{-8}$
Ground resistance (Ω)	0.2
Separation between phases (cm)	42.5
L_1(m)	540
L_2(m)	600
L_3(m)	660
Load current for the simulations (A)	1200
Power factor	1

$$\left.\begin{aligned}
I_{oa} &= J_{l1} - I_{11L} - I_{12L} - I_{13L} \\
I_{ob} &= J_{l2} - I_{21L} - I_{22L} - I_{23L} \\
I_{oc} &= J_{l3} - I_{31L} - I_{32L} - I_{33L} \\
I_{1a} &= (J_{l1} + I_{11R} - I_{12L} - I_{13L}) - (J_{l2} + I_{21R} - I_{22L} - I_{23L}) \\
I_{1b} &= (J_{l2} + I_{21R} - I_{22L} - I_{23L}) - (J_{l3} + I_{31R} - I_{32L} - I_{33L}) \\
I_{1c} &= (J_{l3} + I_{31R} - I_{32L} - I_{33L}) - (J_{l1} + I_{11R} - I_{12L} - I_{13L}) \\
I_{2a} &= (J_{l1} + I_{12R} + I_{11R} - I_{13L}) - (J_{l2} + I_{21R} + I_{22R} - I_{23L}) \\
I_{2b} &= (J_{l2} + I_{21R} + I_{21R} - I_{23L}) - (J_{l3} + I_{32R} + I_{31R} - I_{33L}) \\
I_{2c} &= (J_{l3} + I_{31R} + I_{32R} - I_{33L}) - (J_{l1} + I_{11R} + I_{12R} - I_{13L}) \\
I_{ea} &= J_{l1} + I_{11R} + I_{12R} + I_{13R} \\
I_{eb} &= J_{l2} + I_{21R} + I_{22R} + I_{23R} \\
I_{ec} &= J_{l3} + I_{31R} + I_{32R} + I_{33R}
\end{aligned}\right\} \quad (7)$$

B. Study Cases/Cable Modeling

A 220 kV CB cable system with the parameters stated in Table I, was modeled using the ATP software. The implemented cable system model corresponds to the equivalent pi-model of a three phase cable system of three conductors and three cable sheaths. The pi-model parameters are obtained from the geometrical and electrical parameters of the cable taking into account the earth return impedance. The resistance and the capacitance of the cable per unit length are obtained from the datasheet of the manufacturer. The geometrical equivalent radius of the conductor is considered as if it were formed by a solid cylinder as well as, the equivalent radius of the sheath is determined as if it were formed by a ring, instead of by cylindrical wires (cable strands). Using these parameters, the equivalent resistivities of the conductor and the sheath per unit length are determined. Similarly, the equivalent relative permittivity of the insulation is determined in order to keep the capacitance per unit length equal to the one given in the data sheet. Fig. 5 shows the implemented circuit model on the ATP software. Each box represents one minor section. The resistances marked with *f* have a negligible value and are used to connect the three phase sheath to ground. Furthermore, a model based on the analytical equations, stated in the previous subsection, was applied using the mathematical software Matlab. The cable was modeled in flat formation in a CB configuration with and without transposition and in trefoil formation without transposition.

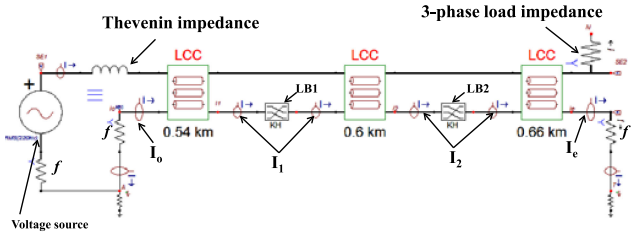

Fig. 5. Cable circuit model on ATP software.

TABLE II
(A) COMPARISON BETWEEN ATP AND MATLAB RESULTS FROM THE SENSORS AT THE TERMINALS UNDER NORMAL CONDITIONS. (B) COMPARISON BETWEEN ATP AND MATLAB RESULTS FROM THE SENSORS AT LINKBOXES UNDER NORMAL CONDITIONS

(A)

Location of sensors		Beginning terminal			Ending terminal		
Sensors (A)		I_{oa}	I_{ob}	I_{oc}	I_{ea}	I_{eb}	I_{ec}
Flat formation in CB without transposition	ATP	70.0	47.6	60.9	46.5	60.2	70.0
	Matlab	68.0	50.5	59.3	50.5	59.3	68.0
Flat formation in CB with transposition	ATP	55.3	54.9	64.0	55.0	54.3	64.2
	Matlab	54.8	54.3	64.7	54.4	53.7	63.5
Trefoil formation	ATP	53.1	53.1	52.5	52.5	52.5	52.5
	Matlab	53.0	53.0	53.0	52.4	52.4	52.4

(B)

Location of sensors		Linkbox1			Linkbox1		
Sensors		I_{1a}	I_{1b}	I_{1c}	I_{2a}	I_{2b}	I_{2c}
Flat formation in CB without transposition	ATP	114	78.4	78.5	87.3	123	121
	Matlab	114	79.0	79.0	87.6	122	121
Flat formation in CB with transposition	ATP	115	114	97.3	105	106	89.0
	Matlab	115	114	98.0	105	106	89.4
Trefoil formation	ATP	93.0	93.0	93.0	101	101	101
	Matlab	93.3	93.3	93.3	101	101	101

A comparison between ATP and Matlab models is performed to check both of them. As it is shown in Tables II.a and II.b, a good agreement between the results obtained applying the analytical equations and those calculated with ATP is achieved. The ATP model takes into account the effect of both the capacitive and inductive currents simultaneously by means of the impedance and admittance matrices while in the programed Matlab model, the inductive and capacitive components of the total sheath currents are calculated separately and later the superposition is applied to calculate the total sheath current. For this reason, the values obtained from the ATP model are considered to be more accurate and thus, they are regarded as the reference values [14].

The results also indicate that the sheath currents in CB configuration with transposition of flat formation are smaller than those without transposition. Therefore, it can be corroborated in this paper that cable transposition should be used for CB in flat

TABLE III
CRITERION OF DEFECT CLASSIFICATION

Condition	Classification	Level
$Is \leq 0.75pu$	Below the normal expected value	#0
$0.75pu < I_s \leq 1.25pu$	Normal expected value	#1
$1.25pu < I_s \leq 7.5pu$	Above the normal expected level	#2
$7.5pu < I_s \leq 12.5pu$	Very above the normal expected level	#3
$12.5pu < I_s$	Ultra above the normal expected level	#4

formation, while it is not required for CB in trefoil formation, in which the smallest sheath currents are achieved.

C. Defect Detection Criterion by the Total Induced Current in the Cable Sheath

A general criterion for detecting defects in cable sheath was introduced in [8] on the basis of the total induced current in the cable sheath (TICS). The TICS in each sensor is expressed in per-unit being referred to its expected value in the normal operation condition (no defect). The resulted values are classified into 4 discrete levels #0, #1, #2, #3 and #4 (see Table III), each level represents a change in the sheath current (I_s) in case of defect with respect to the expected current for normal operation (no defect).

Level #1 is used to represent the current level in normal conditions (no defect) with a tolerance of 25%, taking into account the influence parameters such as: percentage of unbalance in the minor sections, load current, cable characteristics, measuring uncertainties, temperature effect etc. The transition limit between level #2 and #3 (7.5 pu) and between #3 and #4 (12.5 pu) are chosen with an order of magnitude greater (10 times) than the threshold to pass from #0 to #1 and from #1 to #2.

A Simple operation code (SOC) is obtained to identify different types of defects that might occur in the cable sheath through 12 digits. The first set of three digits represents the currents measured by the sensors located at the beginning terminal T_o (I_{oa}, I_{ob}, I_{oc}), the second set of three digits corresponds to the currents at the ending terminal T_e (I_{ea}, I_{eb}, I_{ec}). The third set corresponds to the currents at the first linkbox C_1 (I_{1a}, I_{1b}, I_{1c}) and the last set to the currents at the second linkbox C_2 (I_{2a}, I_{2b}, I_{2c}). The SOC is split in two sub-SOCs, terminal code C_o, C_e and cross code C_1, C_2.

For low load currents the percentage of the inductive current in the total current decreases, while the percentage of the capacitive current increases. This effect leads to the instability of the diagnostic codes, obtained from TICS, under low levels of load current. In order to mitigate this effect, a complementary method on the basis of subtracting the current induced due to capacitive coupling is proposed.

D. Improved Defect Detection Criterion

The capacitive current subtraction (CCS) proposed method allows obtaining only the inductive current (J_{l1}, J_{l2} and J_{l3}) in each cable sheath loop by subtracting the capacitive current. The capacitive current component is obtained by ATP considering a zero load current. Alternatively the inductive current can be also determined by assuming a negligible relative permittivity. Both

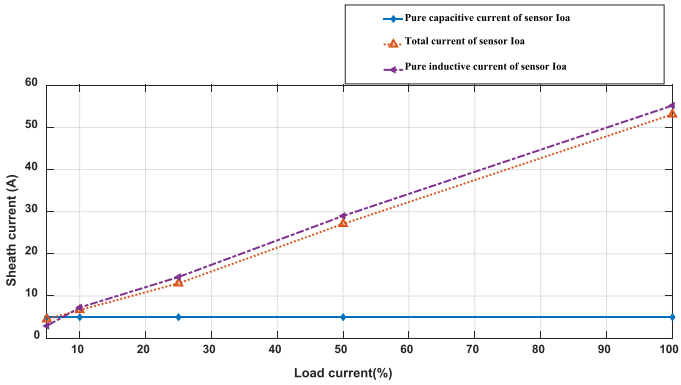

(a)

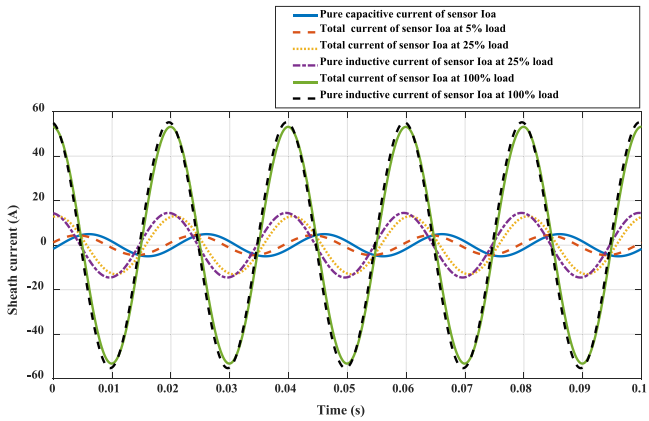

(b)

Fig. 6. (a) Relation between sheath currents and load currents. (b) Influence of high and low load current levels on sheath currents.

procedures permit to verify if the inductive current is correctly determined when the CSS method is applied. Fig. 6(a) indicates the pure capacitive, pure inductive and the total cable sheath current that are obtained from sensor I_{oa} at different percentages of load current. In Fig. 6(a) it can be noticed, the almost direct proportionality between the total circulating current in the sheath and the inductive current with the load current, where the capacitive component is too small and does not depend on the load current (remains constant). Fig. 6(b) shows the phase displacement of the total induced current in the cable sheath (I_{oa}), which is nearly equal to the inductive current for high load currents, while it is close to the capacitive current for low levels of load current.

The SOC that will be obtained after applying the CCS method, are based on the calculations of the per unit values of the total induced current detected by a sensor, under a certain defect (I_d) subtracted from the capacitive current detected by the same sensor under the same defect (I_{dc}). This value is divided by the expected value of the total induced current under normal condition at a certain load level (I_N), subtracted from the capacitive current under normal condition (I_{Nc}), as shown in (8). It is important to note that this method requires phasor sheath current measurements.

$$I_{p.u} = \frac{I_d - I_{dc}}{I_N - I_{Nc}} \tag{8}$$

TABLE IV
SOC UNDER OPEN CIRCUIT FAULT IN SHEATH LOOP

Location	Formation	Load current (%)	$C_o, C_e / C_1, C_2$ TICS
Loop1	Trefoil	100-25	011,110/001,100
	Flat	100-25	011,011/100,100
Loop 2	Trefoil	100-25	101,011/100,010
	Flat	100-25	101,101/010,010
Loop 3	Trefoil	100-25	110,101/010,001
	Flat	100-25	110,110/001,001

Where,

I_d is the sheath current in case of a defect,
I_{dc} is the capacitive component of I_d,
I_N is the sheath current in normal condition (no defect) and
I_{Nc} is the capacitive component for the I_N.

III. TYPES OF DEFECTS

This section is dedicated to show different types of defect that may occur in the cable sheaths and how these defects affect the diagnostic codes C_o, C_e and C_1, C_2. The criterion presented in Section II is used for the analysis. The evaluation is initially performed assuming that the load current is 100% (1200 A for the studied case) which is not usually reached in the normal operation of a real cable.

The influence of reducing the load current on the diagnostic codes, obtained from TICS C_o, C_e and C_1, C_2 is also studied in this section. The values of the diagnostic codes are also shown after applying the CCS method. The cable used for this analysis, has the parameters stated in Table I.

A. Open Circuit Fault in Sheath Loop

This type of defect occurs when a sheath is disconnected to ground. It is assumed that the defect might present at different positions along each loop (T_o, LB_1, LB_2 and T_e) see Figs. 3 and 4. Table IV shows the codes obtained from the sensors located at the terminals (C_o, C_e) and at the linkboxes (C_1, C_2) in case of occurrence of open circuit defect at different loops. It is important to note that same SOC is obtained independently on the location of the open circuit along the same sheath loop.

By applying the TICS method, presented in Subsection II.C, on this defect, a good stability is maintained up to 25% of the applied load current (see Table IV). A significant instability of the codes appears for lower load currents even when an open circuit fault occurs along the same loop. Table V shows the instability of the codes at 17% and 5% of load current when the disconnection occurs at different positions along loop1.

However, by applying the CCS method, the stability is maintained for load currents from 5% to 100% (see the last two columns in Table V). It is important to note that if the open circuit occurs at the cable terminals independently on the load current applied, the sheath current measured by the sensors placed in those positions will be zero, which permits the localization of this defect at once.

TABLE V
INFLUENCE OF LOW PERCENTAGE OF LOAD CURRENT ON THE SOCS

Cable formation	defect along loop1	I_{Load} (%)	$C_o, C_e/C_1, C_2$ TICS	$C_o, C_e/C_1, C_2$ CCS
Trefoil	T_o	17	011,010/011,100	011,110/001,100
		5	011,110/221,101	
	LB_1	17	001,011/001,100	
		5	111,111/001,111	
	LB_2	17	001,011/011,100	
		5	111,111/221,100	
	T_e	17	011,010/011,101	
		5	011,110/221,101	
Flat	T_o	17	011,011/100,011	011,011/100,100
		5	011,011/122,110	
	LB_1	17	001,001/100,010	
		5	101,101/100,111	
	LB_2	17	001,001/100,011	
		5	111,111/122,010	
	T_e	17	011,011/101,010	
		5	011,011/122,110	

TABLE VI
SOC UNDER BREAKDOWN BETWEEN SHEATHS IN TREFOIL FORMATION (CB WITHOUT TRANSPOSITION)

Location of defect	load current (%)	$C_o, C_e/C_1, C_2$ TICS	$C_o, C_e/C_1, C_2$ CCS
LB_{1a}	100-25	414,133/223,232	414,133/223,232
	17	414,122/223,222	
	5	313,122/324,222	
LB_{1b}	100-25	441,313/322,222	441,313/322,222
	17	441,212/322,222	
	5	331,212/432,222	
LB_{1c}	100-25	144,331/232,322	144,331/232,322
	17	144,221/232,222	
	5	133,221/243,222	
LB_{2a}	100-25	133,441/223,232	133,441/223,232
	17	122,441/223,222	
	5	122,331/324,222	
LB_{2b}	100-25	313,144/322,222	313,144/322,222
	17	212,144/322,222	
	5	212,133/432,222	
LB_{2c}	100-25	331,414/232,322	331,414/232,322
	17	221,314/232,222	
	5	221,313/243,222	

From Tables IV and V, it is noticed that by applying the improved CCS method the defect can be detected and localized either at the terminal or at the linkboxes for load current greater than 5%.

B. Breakdown Between Two Sectionalized Sheaths

When the insulation of the coaxial cables used to connect the sheaths to each other fails or when the insulation between sectionalized sheaths of the joint fails, a short circuit between two sheaths occurs.

This fact leads to an increase in the current to be measured by the sensors and forms the codes presented in Tables VI and VII. This kind of defect has been implemented with the ATP software by interconnecting a very small resistance (10^{-8} ohm) between the metal sheaths coming from a certain cable joint.

TABLE VII
SOC UNDER BREAKDOWN BETWEEN SHEATHS IN FLAT FORMATION (CB WITH TRANSPOSITION)

Location of defect	Load current (%)	$C_o, C_e/C_1, C_2$ TICS	$C_o, C_e/C_1, C_2$ CCS
LB_{1a}	100-25	414,313/343,232	414,313/343,232
	17	414,312/243,232	
	5	313,212/232,243	
LB_{1b}	100-25	144,132/433,322	144,132/433,322
	17	144,132/322,322	
	5	133,122/222,333	
LB_{1c}	100-25	441,331/324,223	441,331/324,223
	17	441,331/224,223	
	5	331,221/223,234	
LB_{2a}	100-25	313,414/232,232	313,414/232,232
	17	313,413/222,232	
	5	212,312/222,243	
LB_{2b}	100-25	132,144/322,322	132,144/322,322
	17	132,133/222,322	
	5	122,122/212,433	
LB_{2c}	100-25	331,441/223,223	331,441/223,223
	17	331,441/222,223	
	5	221,231/122,234	

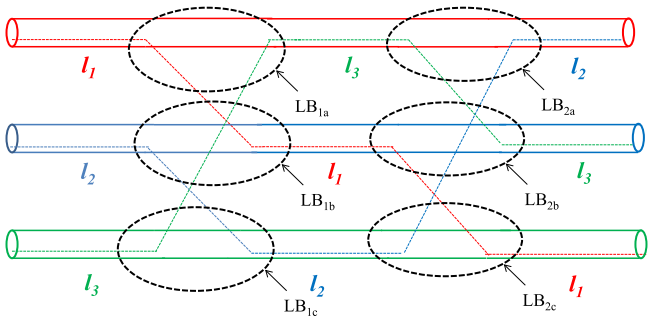

Fig. 7. Geometrical sectionalized sheaths in CB configuration without transposition (trefoil formation).

Fig 7 shows the geometrical sectionalization of sheaths in a CB configuration without transposition.

Although the cable sheaths in a cable joint of a CB configuration with transposition maintain their continuity (electrical position), they are physically sectionalized as shown in Figs. 4 and 8. This is done in order to return the cable sheaths to their original position. A breakdown between two sectionalized sheaths is critical in a CB with and without transposition as well.

Tables VI and VII show the SOCs obtained from the current detected in each sensor for different percentages of load current in trefoil formation (CB without transposition) and in flat formation (CB with transposition) respectively. By analyzing the results shown, it can be noticed that the codes C_o, C_e and C_1, C_2 are changeable according to the position where the defect occurs, which permits detecting and localizing the defect easily either in flat or trefoil formation. After applying the CCS method, the codes maintain the stability at low levels of load

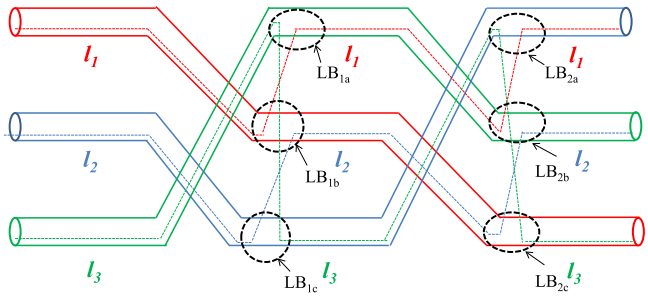

Fig. 8. Geometrical sectionalized sheaths in CB configuration with transposition (flat formation).

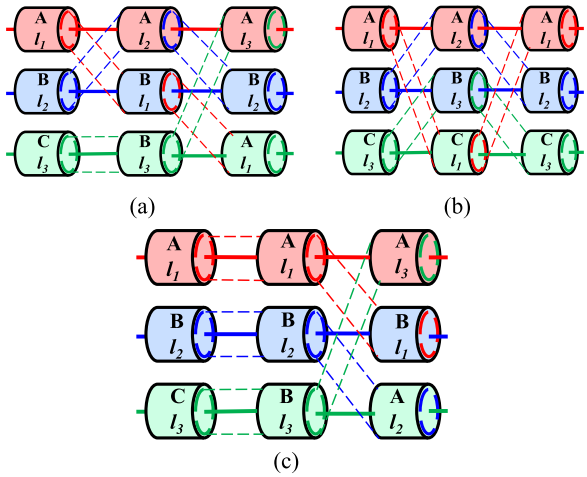

Fig. 9. Wrong sheath connection scenarios in trefoil formation (a) scenario 1 (b) scenario 2 (c) scenario 3.

current. Consequently, the CCS method is more efficient than the simple operation code method.

C. Defect of Installation in Linkbox

This section is focused on showing different scenarios of wrong sheath connections in linkboxes and their effect on the sheath currents. As in this paper the flat and trefoil formations have different CB configurations (with and without transposition), several scenarios can occur in each one of them. Fig. 9 shows the erroneous sheath connection scenarios that were studied for trefoil formation (see Fig. 2(a)), while Fig. 10 shows those studied scenarios for flat formation (see Fig. 2(b)). Table VIII shows the codes obtained from both configurations for different percentages of load current, before and after applying CCS method.

Due to the high values obtained in the sheath currents caused by these defects, the codes obtained from TICS maintain the stability up to 17% of the load current at some scenarios e.g., scenario 4 and 6. Whereas after applying the CCS method, the codes maintain the stability for a wide range of load current up to 5% for all the studied scenarios.

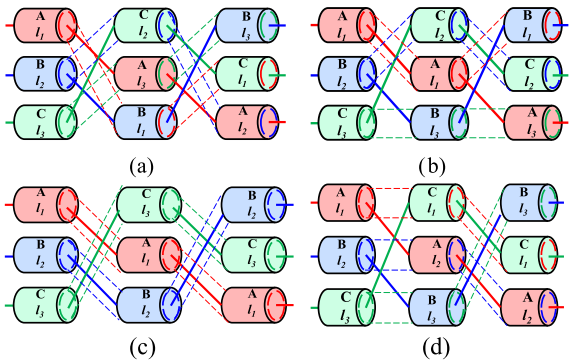

Fig. 10. Wrong sheath connection scenarios in flat formation (a) scenario 4 (b) scenario 5 (c) scenario 6 (d) scenario 7.

TABLE VIII
SOC UNDER WRONG CONNECTION IN LINKBOX

Defect scenario	Load current (%)	$C_o, C_e/C_1,C_2$ TICS	$C_o, C_e/C_1,C_2$ CCS
Scenario 1	100-17	133,331/220,322	133,331/220,322
	5	122,221/330,222	
Scenario 2	100-17	333,333/333,333	333,333/333,333
	5	222,222/444,222	
Scenario 3	100-25	333,333/000,333	333,333/000,333
	17	333,333/000,222	
	5	222,222/000,222	
Scenario 4	100-5	222,222/222,222	222,222/222,222
Scenario 5	100-25	332,332/223,224	332,332/223,224
	17	332,332/223,234	
	5	221,221/222,234	
Scenario 6	100-17	444,444/444,444	444,444/444,444
	5	333,333/333,444	
Scenario 7	100-25	333,333/333,333	333,333/333,333
	17	333,333/322,433	
	5	222,222/222,444	

D. Flooding in Link Box Defect

Flooding in linkboxes causes a three phase short circuit in linkboxes which leads to an excess in the sheath currents measured. The obtained codes form this defect at different locations along the CB system in trefoil and flat formation are shown in Tables IX and X.

It can be observed that this defect provokes the highest increase in the sheath currents. As a result of that, it is observed that C_o in trefoil formation and C_o, C_e in flat formation maintain stability till 17% of load current. Nevertheless, to guarantee the stability of the SOC obtained from all the measuring points, CCS method has to be applied.

E. Actual Values of Sheath Current in Case of Defect

This section is devoted to show actual values of sheath current in case of defect. Table XI.a and XI.b show an example

TABLE IX
SOC UNDER FLOODING IN LINKBOXES IN TREFOIL FORMATION

Defect location	Load current (%)	$C_o,C_e/C_1,C_2$ TICS	$C_o,C_e/C_1,C_2$ CCS
LB1	100-25	444,333/333,333	444,333/333,333
	17	444,222/333,222	
	5	333,222/444,222	
LB2	100-25	333,444/333,333	333,444/333,333
	17	333,444/333,222	
	5	222,444/444,222	
LB1&LB 2	100-25	444,444/000,000	444,444/000,000
	17	444,333/000,000	
	5	333,333/111,000	

TABLE X
SOC UNDER FLOODING IN LINKBOXES IN FLAT FORMATION

Defect location	Load current (%)	$C_o,C_e/C_1,C_2$ TICS	$C_o,C_e/C_1,C_2$ CCS
LB1	100-25	444,333/444,333	444,333/444,333
	17	444,333/343,333	
	5	333,222/232,444	
LB2	100-25	333,444/333,333	333,444/333,333
	17	333,444/222,444	
	5	444,444/343,444	
LB1&LB 2	100-25	444,444/444,444	444,444/444,444
	17	444,444/343,444	
	5	333,333/232,444	

TABLE XI
(A) SIMULATED SHEATH CURRENTS DETECTED FROM THE SENSORS AT TERMINALS. (B) SIMULATED SHEATH CURRENTS DETECTED FROM SENSORS AT LINKBOXES

(A)

Type and location of the defect	Beginning terminal			Ending terminal		
	I_{oa} (A)	I_{ob} (A)	I_{oc} (A)	I_{ea} (A)	I_{eb} (A)	I_{ec} (A)
Open circuit fault at T_{oa}	0	23.3	23.3	22.4	23.7	0.84
Breakdown at LB_{1a}	428	26.9	445	26.6	205	221
Installation defect in LB Scenario 2	234	234	234	228	228	228
Flooding at LB1	411	411	411	200	200	200
Normal operation	27.1	27.1	27.1	26.6	26.6	26.6

(B)

Type and location of the defect	Linkbox 1			Linkbox 2		
	I_{1a} (A)	I_{1b} (A)	I_{1c} (A)	I_{2a} (A)	I_{2b} (A)	I_{2c} (A)
Open circuit fault at T_{oa}	16.5	31.4	47.6	55.9	26.8	32.2
Breakdown at LB_{1a}	218	236	455	198	436	246
Installation defect in LB Scenario 2	398	398	398	406	405	406
Flooding at LB1	452	452	452	436	436	436
Normal operation	47.6	47.6	47.6	55.9	55.9	55.9

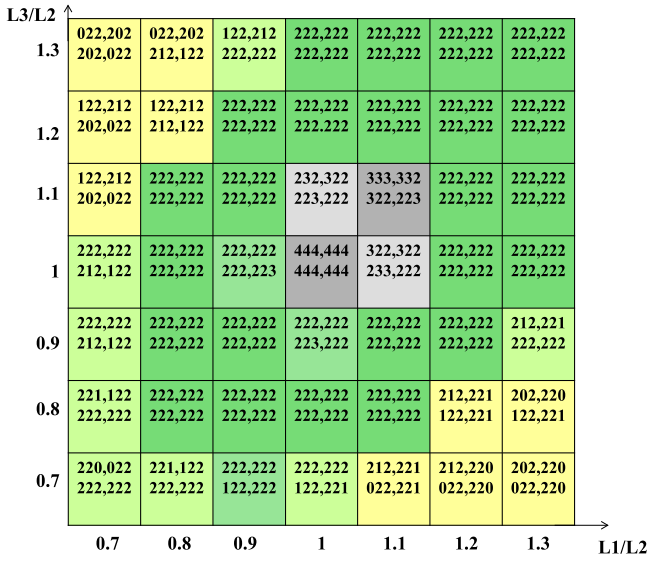

Fig. 11. Influence of the percentage of unbalance on the SOCs.

TABLE XII
TENDENCY OF CHANGE IN SOCS UNDER DIFFERENT COMBINATIONS OF UNBALANCE IN MINOR SECTIONS

Tendency of change in SOC		Percentage from the total number of possible combinations (%)	Highlighted color in Fig. 11
a)	Maintains constant	48.9	Dark green
b)	Varies in one digit of one sub-SOC	6.00	Medium green
c)	Varies in two digits of one sub-SOC and maintains in the other	16.0	Light green
d)	Maintains at least one sub-SOC (a + b + c)	71.4	Green
e)	SOCs change to lower values	20.4	Yellow
f)	SOCs change to higher values	8.10	Grey
g)	Vary in more than two digits in both sub-SOCs (e + f)	28.6	Yellow and grey

for each of the defects studied in this paper when trefoil formation under 50% of load current is considered. The cable used for these calculations has the parameters stated in Table I. The currents under normal operation are indicated in the last row of the tables. It is noticed that the sheath currents increase in all the studied defects except in case of open circuit fault, where they decrease.

IV. UNBALANCE IN MINOR SECTIONS INFLUENCE

This section is devoted to show the influence of the percentage of unbalance in the minor sections of a CB cable system under 100% of load current. The study in this section is started by taking the length of the middle section as the reference length. Whilst the lengths of the other two sections are considered as a percentage of the reference length (the length of the middle section), assuming $\pm 30\%$ is the highest percentage of unbalance that might occur in a CB cable system [5]. This percentage is assumed according to [5], for the worst unbalance that might occur in a CB configuration when taking into account the installation circumstances that may affect the lengths in the minor sections in CB configurations. As the percentage of unbalance increases, the circulating current in the cable sheath increases. This might affect the SOC obtained. Fig. 11 illustrates the code obtained at almost all the possible combinations of unbalance that might occur in a CB cable system, in case of inadequate sheath connection in linkbox scenario 4. Table XII shows the tendencies of change in the SOC with respect to the one obtained in Table VII and their percentages from the total number of unbalance combinations that might occur in CB configuration.

From Fig. 11, it can be observed that there is a diagonal symmetry in the codes obtained from transposal values of L1/L2 and L3/L2, in terms of the tendency of change in the sheath currents. For example, the code obtained for L1/L2 = 0.9 and L3/L2 = 1.2 is the same as the one obtained for L1/L2 = 1.2 and L3/L2 = 0.9. In the same way, the code obtained for L1/L2 = 1.3 and L2/L3 = 0.7 have the same decreasing tendency as the code obtained for L1/L2 = 0.7 and L2/L3 = 1.3 (022,202, 202,022), which means that in all measurement positions the current decreases in one phase.

In case that the percentage of unbalance between the minor sections exceeds 30%, for example $\pm 40\%$, the probability of instability in the codes increases.

V. GENERALIZATION

It has been shown that in case of open circuit fault in the sheath loop, the sheath current decrease contrary to the rest of the cases where the sheath currents increase. Consequently, the codes obtained in case of open circuit in sheath loop are between #0 and# 1. However, in case of occurrence of any of the other types of defects, the sheath current increases which lead to codes #2, #3 and #4. In all the defects studied in this paper, the code digits are changeable according to the location of the defect.

Consequently, the flow chart illustrated in Fig. 12 is defined to detect and localize cable sheath defects. This flow chart starts by measuring the sheath current with all the sensors (I_{ok}, I_{1k}, I_{2k} and I_{ek}) where k = a, b and c. If one of the sensors at the terminal I_{ok} or I_{ek} measures approximately zero, then the identification and localization of the open circuit fault is possible, considering the position of the sensor that measures approximately zero. Otherwise, the TICS method can be applied as long as the load current is greater than 25%. If the obtained codes are composed of zeros and ones, then the defect is identified to be open circuit fault at the joints. On the other hand, if the obtained code is a standard code as those presented in Section III, the defect can be identified.

However it is important to note that in flat formation, the produced code from flooding defect in both linkboxes (see Table X) and the one produced from the inadequate connection in linkboxes scenario 6 (see Table VIII) are the same. Thus

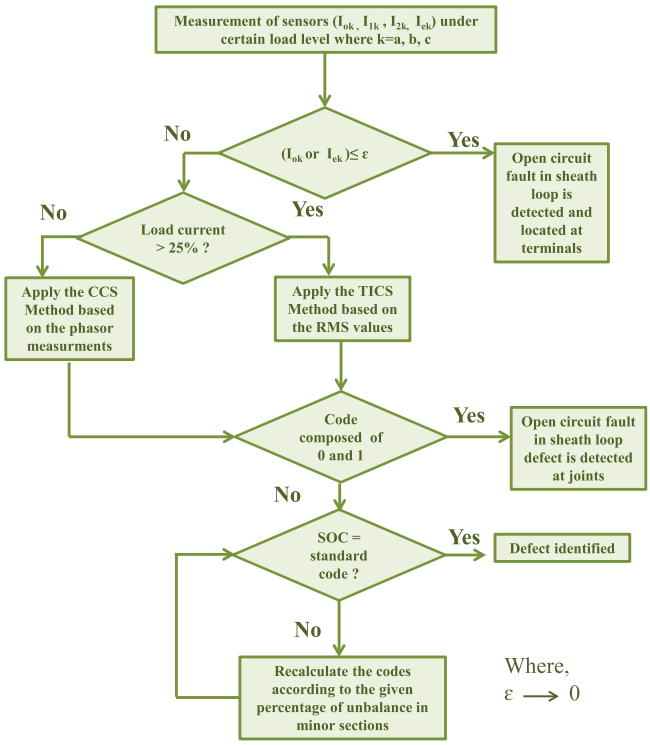

Fig. 12. Flowchart of the detection method.

TABLE XIII
PARAMETERS OF THE MEASURED CABLE

Parameters	Value
Equivalent radius of the conductor (mm)	21
Equivalent internal sheath raduis(mm)	38.6
Equivalent external sheath raduis (mm)	42
Equivalent sheath resistivity(Ω·m)	$2.2.10^{-7}$
Sepation distance (cm)	30

in this particular case, one can distinguish between both defects by just checking the linkboxes visually. For low levels of load current, it is recommended to apply the CCS method. Otherwise the SOCs have to be recalculated according to the unbalance in the minor sections in the particular studied case. To guarantee a perfect detection and localization at least measurement at two different locations is required (I_o, I_1, I_2 and I_e sites). However, at some cases, the localization and the identification of the defect can be performed by just measuring at only one location. For example: in case of breakdown between sheaths at LB_{1a} in trefoil formation (Table VI), by just obtaining the measurements at I_o (C_o, 414), the defect can be identified and localized due to the unrepeatability of the code in the other studied defects (see Tables IV–X).

VI. REAL MEASUREMENTS VALIDATION

This section is devoted to show a real study case in order to present the validity of the proposed method under a defected scenario.

A real case study is presented in this section, for a 220 kV cable system and its parameters stated in Table XIII, considering

TABLE XIV
PER-UNIT VALUES BASED ON THE MEASUREMENT RESULTS

Measured sensors	I_{ea}	I_{eb}	I_{ec}
Per unit values	1.9	2.7	2.47
Code	2	2	2

TABLE XV
COMPARISON BETWEEN MEASURED, SIMULATED, AND CALCULATED RESULTS

Sensor	I_{ea} (A)	I_{eb} (A)	I_{ec} (A)
Mean of the measured data ± Standard deviation	34.7±3.4	65.3±5.1	59.8±3.5
ATP simulated results	35.6	65.8	54.4
Matlab calculated results	34	67.5	58.2

the lengths of the minor sections are: L1 = 288 m, L2 = 340 m and L3 = 260 m, i.e., L1/L2 = 0.84 and L3/L2 = 0.76. The cable belongs to the Spanish TSO and it is installed in CB with transposition configuration in flat formation and its sheath currents have been monitored [12]. The measurements were taken only from an ending terminal of a cross bonding configuration (I_e) over 20 days under a maximum load current of approximately 500 A, which is almost 50% of the rated load current that can be applied. All the measurements have been normalized to 500 A of load current. The mean and the standard deviation of the measured data were considered for analysis.

An unexpected increase in the sheath currents was detected. Furthermore, a significant unbalance between different cable sheath currents was observed in the measuring point I_e. The developed criterion of SOC was applied, by means of calculating the per-unit values of the sheath current (in case of defect), obtained via measurements with the base value of the expected sheath current (under normal condition) obtained via simulations as shown in Table XIV. Considering the percentage of unbalance between lengths in minor sections, it was found that the code obtained, corresponds to the inadequate sheath connection scenario 4 illustrated in Figs. 10(a) and 11.

This defect has been simulated by means of ATP software. Also a Matlab code has been implemented using the analytical equations under this defected scenario, in order to compare the results obtained from the measurements with those obtained from the simulations and from the calculations, Table XV shows a good agreement between the measured, simulated and calculated results.

VII. CONCLUSION

This paper proposes a new method for the detection and localization of 4 types of defects that might occur in the cable sheath of a cross bonding configuration. Criterion of codes from #0 to #4 is developed in order to represent the level of change of the sheath current in case of defect. This criterion can be applied at load current of 25% or greater. At low levels of load current (<25%), a complementary method has been presented to remove the capacitive current from the total induced current in the sheath in order to maintain the stability.

The criterion proposed in this paper can be also applied on different percentages of unbalance in the minor sections that might exist in CB cable grounding system. Future work will be published on different real cases under normal and anomalous operations with phasor measurements.

ACKNOWLEDGMENT

The authors would like to thank the Spanish TSO for providing the field data which helped in the development of this paper.

REFERENCES

[1] X. Dong, Y. Yang, C. Zhou, and D. Hepburn, "Online monitoring and diagnosis of HV cable faults by sheath system currents," *IEEE Trans. Power Del.*, vol. 32, no. 5, pp. 2281–2290, Oct. 2017.

[2] M. Li *et al.*, "A novel fault localization method based on monitoring of sheath current in a cross-bonded HV cable system," in *Proc. IEEE Elect. Insul. Conf.*, 2017, pp. 123–126.

[3] Y. Yang, D. Hepburn, C. Zhou, W. Zhou, and Y. Bao, "On-line monitoring of relative dielectric losses in cross-bonded cables using sheath currents," *IEEE Trans. Dielectrics Elect. Insul.*, vol. 24, no. 5, pp. 2677–2685, Oct. 2017.

[4] M. Marzinotto and G. Mazzanti, "The feasibility of cable sheath fault detection by monitoring sheath-to-ground currents at the ends of cross-bonding sections," *IEEE Trans. Ind. Appl.*, vol. 51, no. 6, pp. 5376–5384, Nov./Dec. 2015.

[5] *IEEE Guide for Bonding Shields and Sheaths of Single-Conductor Power Cables Rated 5 Kv Through 500 Kv*, IEEE Standard 575-2014, 2014.

[6] R. Benato, S. Dambone Sessa, R. De Zan, M. Guarniere, G. Lavecchia, and P. Sylos Labini, "Different bonding types of Scilla–Villafranca (Sicily–Calabria) 43-km double-circuit ac 380-kV submarine–land cables," *IEEE Trans. Ind. Appl.*, vol. 51, no. 6, pp. 5050–5057, Nov./Dec. 2015.

[7] P. Simón Comín and F. Garnacho, *Cálculo y diseño de líneas eléctricas de alta tensión*. Madrid, Spain: Ibergarceta, 2011.

[8] A. Khamlichi, M. Adel, F. Garnacho, and J. Rovira, "Measuring cable sheath currents to detect defects in cable sheath connections," in *Proc. 52nd Int. Univ. Power Eng. Conf.*, 2017, pp. 1–6.

[9] Z. Tang *et al.*, "Analysis of significant factors on cable failure using the cox proportional hazard model," *IEEE Trans. Power Del.*, vol. 29, no. 2, pp. 951–957, Apr. 2014.

[10] Z. Tang *et al.*, "Comparison of the Weibull and the Crow-AMSAA model in prediction of early cable joint failures," *IEEE Trans. Power Del.*, vol. 30, no. 6, pp. 2410–2418, Dec. 2015.

[11] *IEEE Standard for the Testing, Design, Installation, and Maintenance of Electrical Resistance Trace Heating for Industrial Applications*, IEEE Standard 515–2011, 2011.

[12] A. Burgos, G. Donoso, and B. García, "Sheath currents monitoring in high voltage isolated cables," in *Proc. Int. Council Large Elect. Syst.*, 2016, Paper B1 209.

[13] F. de Leon, M. Marquez-Asensio, and G. Alvarez-Cordero, "Effects of conductor counter-transposition on the positive-sequence impedance and losses of cross-bonded cables," *IEEE Trans. Power Del.*, vol. 26, no. 3, pp. 2060–2063, Jul. 2011, doi: 10.1109/TPWRD.2011.2123473.

[14] H. Dommel, *EMTP Theory Book*. Vancouver, BC, Canada: Microtran Power Syst. Anal. Corp., 1996.

Marina Adel Shokry was born in Cairo, Egypt, in 1992. She received the B.Sc. and M.Sc. degrees in telecommunication engineering from the German University in Cairo, Cairo, Egypt, in 2014 and 2016, respectively. She is currently working toward the Ph.D. degree in electrical engineering at the Polytechnic University of Madrid, Madrid, Spain. She is also working as a Ph.D. Researcher with the High Voltage Technological Center, LCOE, Madrid, Spain. Her research interests include cable sheath currents, HV cable condition monitoring, and antenna design.

Abderrahim Khamlichi received the B.Sc. degree in industrial engineering and the M.Sc. degree in electrical engineering from the Technical University of Madrid, Madrid, Spain, in 1999 and 2015, respectively, where he is currently working toward the Ph.D. degree in the area of electrical power transmission. He is currently with the High Current Laboratory, High Voltage Technological Center (LCOE-F2I2), Madrid, Spain, and an Electrical Engineer with the R&D&I Department. He is also an Educator with the Department of Electrical Engineering in ETSIDI-UPM.

Fernando Garnacho was born in Madrid, Spain, in 1957. He received the M.Sc. degree in industrial electrical engineering and the Ph.D. degree in electrical engineering from the Polytechnic University of Madrid (UPM), Madrid, Spain, in 1981 and 1986, respectively. He is currently a Professor with the Department of Electrical Engineering of the UPM and the Director of the High Voltage Department of the Central Official Laboratory (LCOE), Madrid, Spain. Dr. Garnacho is the Chairman of the Technical Committee 42 "High Voltage Testing Techniques" of the Spanish Standardization Institute AENOR and is a member of the SC D1 "Materials and Emerging Test Techniques" of CIGRE.

Julio Martínez Malo was born in Morenilla (Guadalajara), Spain, in 1948. He received the B.S. degree and the Ph.D. degree in electrical engineering from Universidad Politécnica de Madrid (E.T.S. de Ingenieros Industriales), Madrid, Spain, in 1978 and 1982, respectively. In 1978, he joined the Department of Automática, Ingeniería Eléctrica y Electrónica e Informática Industrial, Universidad Politécnica de Madrid, where he is presently a Professor. He was the Head of the Laboratory for Electrical Metrology and Calibration, Laboratorio Central Oficial de Electrotecnia, Madrid, Spain, from 1988 to the end of 1992. His current research interests include electrical metrology, analog and digital signal processing, electromagnetic transients, and power systems control.

Fernando Álvarez was born in Madrid, Spain, in 1975. He received the M.Sc. degree in technical electrical engineering and in industrial electrical engineering from the Polytechnic University of Madrid (UPM), Madrid, Spain, and from the University Carlos III of Madrid, Madrid, Spain in 1999 and 2008, respectively. In 2015, he received the Ph.D. degree in electrical engineering from the UPM. His doctoral thesis was developed in the High-Voltage Test Laboratory LAT-UPM. Since 2004, he has been an Associate Professor with the Department of Electrical Engineering, UPM. He has participated in several research projects related with HV electrical insulation diagnosis. His research interests include high-voltage insulating materials and partial discharges measurement.